Magnetic Field-Priority Force Control for Automated Manipulation in Large Workspaces With Reconfigurable Electromagnetic Actuation System

Mingxue Cai ⓘ, *Member, IEEE*, Zhaoyang Qi ⓘ, *Student Member, IEEE*, Yanfei Cao ⓘ,
Xinyu Wu ⓘ, *Senior Member, IEEE*, Tiantian Xu ⓘ, *Senior Member, IEEE*,
and Li Zhang ⓘ, *Fellow, IEEE*

Abstract—**Rapid technological advancements in remote-controlled magnetic robots that operate inside the human body have strongly stimulated the development of magnetic actuation systems owing to their ability to produce demanding magnetic fields and forces. However, the efficient generation of the combined field and force in large workspaces still needs to be improved. To resolve this critical challenge, we first investigated the required number of mobile magnetic sources for a magnetic actuation system to regulate field and force in large workspaces. Subsequently, we demonstrated that a three-electromagnetic-coil configuration can effectively produce the desired field and force. This is achieved through the implementation of a field-priority force control method utilizing three robotic arms. Notably, this method considers Yoshikawa manipulability for each robotic arm, which matters for manipulating magnetic robots in large workspaces. Specifically, we evaluated the force error by sampling 50 different field-force combinations from the workspace. Finally, a reconfigurable electromagnetic actuation system (REMA) was developed by mounting three mobile electromagnetic coils mounted on three independent robotic arms. The effectiveness of the proposed method and platform was demonstrated by actuating a capsule robot in both 2-D and 3-D application scenarios.**

Index Terms—**Autonomy in magnetic manipulation, magnetic field and force control, magnetic robots.**

I. INTRODUCTION

IN the past decade, magnetic actuation has emerged as one of the most promising technologies for the noncontact manipulation of small-scale magnetic robots. The ability to control magnetic field (torque) or/and force at any location within a defined workspace has the potential to enhance manipulation dexterity and precision [1], [2], [3], [4], [5], [6], [7]. When both magnetic fields and forces are simultaneously applied for the autonomous propulsion of a magnetic robot, the robot will impose high requirements on the dexterity of the field and force generated by the magnetic actuation system, particularly when dealing with autonomous manipulations in large workspaces [8], [9], [10], [11], [12], [13].

To achieve control over both the field and force with singularity-free operations at a point, eight stationary electromagnetic coils are required by changing only the electric currents, as demonstrated in the OctoMag system [14]. Furthermore, as stated in [15], reconfigurable magnetic manipulation systems can achieve similar control authority to static systems with fewer inputs. Besides, in [16], it is confirmed that the performances of electromagnetic actuation (EMA) systems are not only affected by the number of coils but also by their configurations. The required number of mobile magnetic sources to generate the desired field and force in large workspaces should be further investigated.

This article has been accepted for inclusion in a future issue of this journal. Content is final as presented, with the exception of pagination.

2   IEEE TRANSACTIONS ON INDUSTRIAL ELECTRONICS

For a system with a single magnetic source input maneuvered by a six-degrees-of-freedom (DOF) robotic manipulator, it is possible to achieve three-DOF force-based position control and two-DOF open-loop heading control of a magnetic robot [17]. This is done by establishing a relationship between the joint velocities of the manipulator and small variations in applied force and the magnetic source's heading. However, it remains challenging to achieve the desired magnetic field and magnetic force control in the task space because one mobile magnetic source configuration cannot control the field's amplitude independent of the magnetic force. Furthermore, this configuration consistently generates a magnetically attractive force between the magnetic robot and the magnetic source. It necessitates the presence of a nonmagnetic restoring force, such as gravity, to maintain system stability. To mitigate the effect of control singularities, the authors introduced a strategy that sacrificed control authority over the capsule's heading to maintain three-DOF force control over the capsule's position when the manipulator approaches a kinematic singularity.

Regarding multimagnet actuation techniques with two independent magnetic sources input manipulated by two robotic arms, Pittiglio et al. [18] presented a novel approach for controlling magnetic field and field gradients to magnetically manipulate a continuum robot containing two orthogonal internal permanent magnets (IPMs) using a dual-arm system. The primary study of this work is that it can control up to eight magnetomechanical DOFs using two magnetic sources. However, it may struggle with situations where the field must be turned off over the entire space around the system. In real scenarios, it is hard to guarantee the IPMs to be always orthogonal, when organized in a serial structure such as a continuum robot.

Note that at least three coils are required for any 3-D field control only by changing the electric current in each coil. The DeltaMag [19] and RoboMag [20] were developed using three mobile coils to enable a relatively large workspace, in which the motions of three coils are actuated by the parallel mechanism and robotic arms, respectively. The magnetic force control is more complicated than the field control, primarily due to the complex mapping of the resultant three-element force to a five-element gradient [21], [22]. Although the DeltaMag and RoboMag utilized three mobile coils to primarily implement desired field control, they have yet to prove effective in combined field and force control. Indeed, it is challenging to design a mobile multicoil system, while providing enough workspace to meet the clinical requirements. Therefore, there is a great motivation for a mobile EMA system with large workspaces to have flexible coil configurations and to minimize the required number of coils simultaneously. The task of extending the design of the three-coil system to achieve simultaneous field and force control remains unresolved. By further developing the idea of a three-coil system to generate arbitrary 3-D fields, the force control can be investigated by changing different coil configurations to search for appropriate gradient distributions. This can be achieved by developing a new EMA system that exploits three coils that are mounted on three six-DOF robotic arms and thus can move in 3-D space in a decoupled way.

In this article, the main reasons for choosing the three-coil configuration include two aspects. First, it allows for generating a 3-D field in any desired direction through precise control of the electric currents in each coil. Second, the movable three-coil configuration generates a rich combination of magnetic fields and gradients while providing a large workspace. Subsequently, a field-priority force control method was introduced to generate a flexible coil configuration to manipulate the desired field and force. Besides, this method considers Yoshikawa manipulability for each robotic arm, which matters for manipulating magnetic robots in large workspaces. Finally, a reconfigurable electromagnetic actuation (REMA) system equipped with three mobile coils mounted on three independent 6-DOF robotic arms was implemented to help validate the effectiveness of our method. The experimental results of navigating a capsule in various scenarios validated the effectiveness of our method and the feasibility of the platform.

II. ANALYSIS OF THE REQUIRED NUMBER OF MOBILE COILS

The motivation behind an EMA platform is to provide the necessary field and force for the manipulation of magnetic robots. In [16], it confirmed that the performances of EMA systems are not only affected by the number of coils but also by their configurations. If a stationary EMA platform is upgraded to a reconfigurable system by enabling the control of the position and orientation of coils, it will be resourceful to perform various tasks while reducing the number of coils required for control. To estimate the required number of mobile magnetic sources to generate the desired magnetic field and force, we conducted the analysis in three different scenarios as follows.

A. One Mobile Magnetic Source

For a system with a single magnetic source input maneuvered by a six-DOF robotic manipulator, it is possible to achieve three-DOF force-based position control and two-DOF open-loop heading control of a magnetic robot [17]. This is done by establishing a relationship between the joint velocities of the manipulator and small variations in applied force and the magnetic source's heading. However, it remains challenging to achieve the desired magnetic field and magnetic force control in the task space because one mobile magnetic source configuration cannot control the field's amplitude independent of the magnetic force. Furthermore, this configuration consistently generates a magnetically attractive force between the magnetic robot and the magnetic source. It necessitates the presence of a nonmagnetic restoring force, such as gravity, to maintain system stability.

B. Two Mobile Magnetic Sources

For a system with two wo independant magnetic sources input (permanent magnets) manipulated by two robotic arms, it can achieve control eight DOFs for a continuum robots containing two orthogonal IPMs [18]. However, in real scenarios, it is hard to guarantee the IPMs to be always orthogonal, when organized in a serial structure such as a continuum robot.
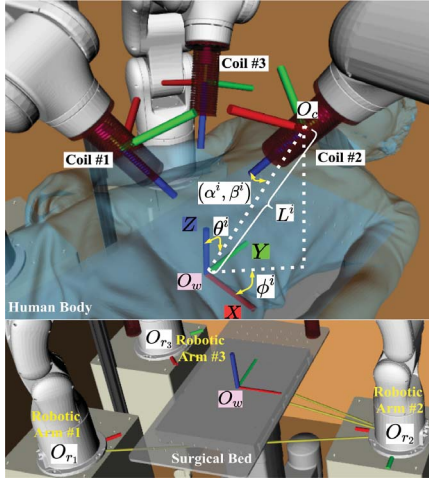
Fig. 1. Definition of optimization parameters to describe a coil pose and relative positions of three robotic arms under the frame O_w. Optimization parameters are described using five elements $(L^i, \theta^i, \phi^i, \alpha^i, \beta^i)$ expressed in the frame O_w. Note that elements of (L^i, θ^i, ϕ^i) denote the spherical coordinates to determine position of the frame O_c. Elements of (α^i, β^i) denote angles that Z-axis of the frame O_c rotates around X-axis and Y-axis of the frame O_c, respectively.

C. Three Mobile Magnetic Sources

For the field control, at least $n = 3$ magnetic sources are required to achieve arbitrary field control in 3-D workspace. For a given magnetic dipole, the induced magnetic force only depends on the magnetic gradient distribution. Note that the magnetic gradient is a variation in the magnetic field $\mathbf{b}(\mathbf{p}_w)$ with respect to a position $\mathbf{p}_w$. When employing a mobile EMA system with three coils, field control can be achieved by changing each coil current. The force control can be investigated by changing different coil configurations to search for appropriate gradient distributions. In fact, it is challenging to design a mobile multicoil system, while providing enough workspace to meet the clinical requirements. Therefore, there is a great significance for a mobile EMA system with large workspaces to have flexible coil configurations and to minimize the required number of coils simultaneously. In the following section, we will report the detailed solution to achieve field and force control in large workspaces.

III. FIELD-PRIORITY FORCE CONTROL METHOD

In this section, we aim to find the pose of three coils (i.e., coil configuration) and corresponding electric currents to manage the desired magnetic field and force. To achieve this goal, we describe the concept of a REMA system based on three six-DOF robotic arms manipulating three coils in a large workspace, as shown in Fig. 1.

A. Problems

Note that each coil provides a total of six DOFs for control: a five-DOF pose (neglecting the coil rotation along its principal axis) and a one-DOF electric current. However, it is not straightforward for the REMA to manage fields and forces in

TABLE I
POSITION AND ORIENTATION OF EACH ROBOTIC ARM'S BASE RELATIVE TO WORLD FRAME

	X(m)	Y(m)	Z(m)	Angle around Z($^\circ$)
Robotic arm #1	−0.470	−0.310	−0.115	45
Robotic arm #2	0.580	0	−0.115	180
Robotic arm #3	−0.470	0.310	−0.115	−45

TABLE II
CONSTRAINTS OF OPTIMIZATION PARAMETERS ($i = 1, 2, 3$)

	L^i(m)	θ^i($^\circ$)	ϕ^1($^\circ$)	ϕ^2($^\circ$)	ϕ^3($^\circ$)	α^i($^\circ$)	β^i($^\circ$)
x_0	0.15	45	225	0	130	0	0
x_{min}	0.11	30	195	−45	90	−18	−18
x_{max}	0.25	60	270	45	165	18	18

the task space due to the complexity of explicitly expressing the mapping from the field and force to the coil configuration and electric currents. Furthermore, to achieve field and force control effectively in a large workspace, it is crucial to take into account the manipulability of the each robotic arm to avoid singularities. Aiming at multiple evaluation metrics that need to be improved, we explore the application of multiobjective optimization (MOO) [23] technique for managing multiobjective functions. In the following subsection, we focus on the design of evaluation metrics and the utilization of the MOO technique to address our problem.

B. Definition of CCS

To evaluate the feasibility of MOO for addressing our problem, a search space, referred to as a CCS, needs to be constructed. For this purpose, we present the definition of the world frame O_{w-xyz} and the coil frame O_{c-xyz} to describe the coil configuration, as illustrated in Fig. 1. The overall configuration of the three robotic arms should provide sufficient space for the operating room bed and imaging system. Hence, we adopted a configuration in which two robotic arms were installed on one side of the bed, and a third robotic arm was placed on the other side (see Table I).

The pose of each coil frame were defined using five elements $\{\mathbf{x}^i = (L^i, \theta^i, \phi^i, \alpha^i, \beta^i) \in \mathcal{R}^5, i = 1, 2, 3\}$ with respect to the world frame. Moreover, certain constraints must be designed for these parameters to obtain a collision-free coil pose (see Table II). For instance, we imposed bounds $(L^i \in (L^i_{min}, L^i_{max}))$ on parameter L^i based on the practical scenario to ensure the position of each coil is always in a safe distance.

We regarded the set of pose parameters of the three coils as the CCS. The CCS $\mathcal{X}$ for an optimization problem is defined as follows:

$$\mathcal{X} := \{\mathbf{x} = (L^1, \theta^1, \phi^1, \alpha^1, \beta^1, \ldots, L^3, \theta^3, \phi^3, \alpha^3, \beta^3) \in \mathcal{R}^{15}\}. \tag{1}$$
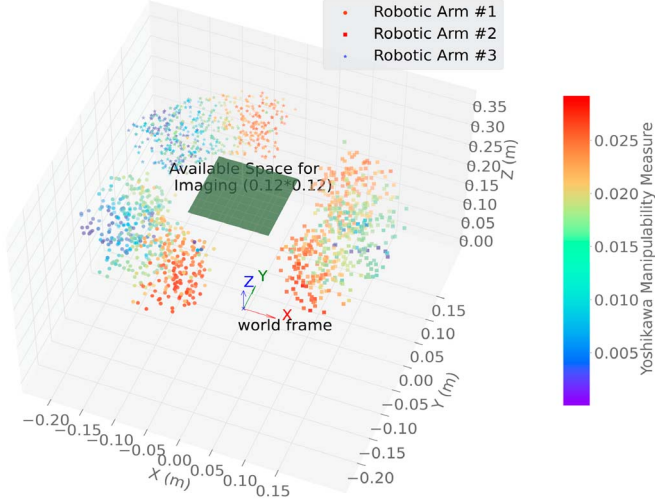
Fig. 2. Distributions of three coils in the workspace with three robotic arms' Yoshikawa manipulability measure.

C. Method

It is worth noting that any 3-D field control can be achieved by the three coils using only the change in their electric currents. Therefore, the field control for our platform can always be guaranteed, provided a set of admissible electric currents ($\mathbf{i}_d \in [-10, 10]$ A). Exploring force control can be achieved by adjusting various coil configurations. Additionally, considering the field and force controls in large workspaces, ensuring each robotic arm has robust manipulability is critical to avoid singularities in a certain joint configuration. Therefore, the Yoshikawa manipulability measure for each robotic arm is considered. Consequently, for a given field and force, the proposed field-priority force control method can guarantee field control and optimize the actual force to a given value with acceptable errors while enhancing Yoshikawa manipulability measure for each robotic arm.

Leveraging the ideas of MOO technology, we formulated the field-priority force control method to simultaneously minimize the force error and maximize each robotic arm's Yoshikawa manipulability measure. Therefore, the MOO problem can be formulated as follows:

$$\mathbf{x}^* = \underset{\mathbf{x} \in \mathcal{X}}{\arg\max} \{e_\mathbf{f}, m_1, m_2, m_3\}$$
$$\text{s.t.} \quad \mathcal{X}_{\min} \leq \mathcal{X} \leq \mathcal{X}_{\max} \qquad (2)$$

where $e_\mathbf{f} = -\|\mathbf{f}_d - \mathbf{f}_a\|$, $\mathbf{f}_d$ denotes the desired force, and $\mathbf{f}_a$ represents the actual force for a specific coil configuration $\mathbf{x}$. The Yoshikawa manipulability $m_i = \sqrt{\det(\mathbb{J}_i(\mathbf{q})\mathbb{J}_i^T(\mathbf{q}))}$, $i = 1, 2, 3$, which describes how well-conditioned the robotic arm is to achieve an arbitrary velocity in the Cartesian space. $\mathbb{J}(\mathbf{q})$ represents the Jacobian matrix of the robotic arm, which is a function of the joint position vector $\mathbf{q}$.

Fig. 2 shows the three-coil spatial distribution and the corresponding Yoshikawa manipulability measure of each robotic arm under the given robotic arm's base position (Table I) and three-coil constraints (Table II). The shape of manipulability of

---

Algorithm 1: Field-Priority Force Control Method

Input: Target position $\mathbf{p}_w$, desired field $\mathbf{b}_d(\mathbf{p}_w)$, desired force $\mathbf{f}_d(\mathbf{p}_w)$.

Output: The Pareto-optimized coil configuration $\mathbf{x}^*$ and electric currents $\mathbf{i}_d$

1 **for** *optimization loop k=1 to K* **do**
2   Sample a set of parameters $\mathbf{x}$ from $\mathcal{X}$ according to (1);
3   Compute each coil's pose with respect to the $\mathbf{p}_w$ using the sampled parameter $\mathbf{x}$;
4   Obtain the field generated by each coil with 1A current at $\mathbf{p}_w$ and construct the actuation matrix $\mathbb{A}_b = [\mathbf{b}_1(\mathbf{p}_w), \mathbf{b}_2(\mathbf{p}_w), \mathbf{b}_3(\mathbf{p}_w)]$;
5   Compute the desired electric currents $\mathbf{i}_d$ and apply them to the coils $\mathbf{i}_d = \mathbb{A}_b^{-1}\mathbf{b}_d(\mathbf{p}_w)$;
6   Compute resultant magnetic gradients $\nabla\mathbf{b}(\mathbf{p}_w)$;
7   Compute actual magnetic force $\mathbf{f}_a = (\mathbf{m} \cdot \nabla)\mathbf{b}(\mathbf{p}_w)$;
8   Compute the manipulability for each robotic arm m_i $(i = 1, 2, 3)$;
9   MOO procedure loop via the NSGA-II algorithm to optimize objective function according to (2);
10 **end**
11 Obtain the Pareto-fronts;
12 Normalize $e_\mathbf{f}, m_1, m_2, m_3$;
13 Compute the pseudo-weight according to (3);
14 Obtain the Pareto-optimized coil configuration from Pareto-fronts based on the pseudo-weight.

---

each robotic arm is not symmetrical owing to the unsymmetrical workspace, installation, and sampling. Moreover, during the optimization process, the objective is to place the coils in locations with maximized manipulability as much as possible. Simultaneously, we observed that space is available for imaging magnetic robots to avoid occlusions. The nondominated sorting genetic algorithm (NSGA)-II [24] was chosen as the algorithm for solving the MOO problem due to its capability to explore extensive search spaces, as described in Algorithm 1.

After obtaining the values for the four objective functions ($e_\mathbf{f}, m_1, m_2, m_3$), the NSGA-II algorithm was employed to compute a set of nondominated solutions, known as the Pareto front. It is important to mention that the running time of the NSGA-II algorithm for solving our problem on the REMA platform is approximately 0.5 s and operates online. However, developing a method to narrow down the Pareto front to a single appropriate solution for practical application, which involves selecting an appropriate coil configuration from the obtained set for further control, is challenging. In our study, we selected a solution from the Pareto front using a pseudoweight vector approach. The pseudoweight w_i for the ith objective function can be calculated as follows:

$$w_i = \frac{(f_i^{\max} - f_i(x)) / (f_i^{\max} - f_i^{\min})}{\sum_{m=1}^{M} (f_m^{\max} - f_m(x)) / (f_m^{\max} - f_m^{\min})} \qquad (3)$$

where $f_i^{\max}$ and $f_i^{\min}$ denote the maximum and minimum values of the objective function in obtained Pareto front. This equation calculates the normalized distance to the worst solution for each objective function f_i. Since the four objectives have different scales, Min–Max normalization was applied to perform a linear transformation on the obtained Pareto front. Once a Pareto-optimized coil configuration and corresponding electric currents are obtained, the robotic arms would adjust their poses to reach the Pareto-optimized coil configuration and set the desired coil currents.

D. Feasibility Evaluation

Due to the complexity of the high-dimensional field-priority force control method, it is rather difficult to verify its feasibility, that is, to evaluate whether a magnetic robot can be manipulated with a set of desired fields and forces while staying in any pose during autonomous magnetic manipulation. To simplify the quantitative analysis of the proposed method without loss of generality, we defined a direction vector space for a set of desired fields and forces and then analyzed the feasibility of our proposed method by constructing a direction vector space $\mathcal{S}$ using 50 direction vectors uniformly sampled from the 3-D spaces. Each direction vector is denoted by $\hat{\mathbf{s}}$, such as $\hat{\mathbf{s}} = [1, 0, 0]^T$. Therefore, the $\mathcal{S}$ is intuitively defined as follows:

$$\mathcal{S} = \left\{ \hat{\mathbf{s}} \in \mathcal{R}^3 \right\}. \tag{4}$$

Based on the designed $\mathcal{S}$, we uniformly sampled two direction vectors, namely $\hat{\mathbf{s}}_{\mathbf{b}}$ and $\hat{\mathbf{s}}_{\mathbf{f}}$, from $\mathcal{S}$ to serve as direction vectors for the applied field and force, respectively. It should be noted that the value of dipole moment $\|\mathbf{m}_r\|$ of the magnetic robot only affects the amplitude of the generated force. Hence, we considered the unit dipole moment $\hat{\mathbf{m}}_r$ in our study. Once the two direction vectors are sampled, along with the specified desired field and force amplitudes, the method presented in Algorithm 1 can be used to determine the coil configuration and electric current. Because field control is prioritized and guaranteed during the optimization, we focused on the feasibility of the force generation. We defined an evaluation index in terms of force percentage error ε, to describe the difference between the desired and the actual force, which is given as follows:

$$\varepsilon = \frac{\|\mathbf{f}_d - \mathbf{f}_a\|}{\|\mathbf{f}_d\|} \times 100\% \tag{5}$$

where $\mathbf{f}_d$ and $\mathbf{f}_a$ are the desired and actual force, respectively.

The overall results are presented in Fig. 3. Based on the applied unit dipole moment, the desired fields and forces were employed to observe the obtained actual force under the 50 randomly sampled direction vectors. In Fig. 3(a), where the desired field is 1 mT, we observed the distributions of the force percentage error across the sampled 50 direction vectors within the desired force range [5 and 100 mN] in the defined CCS $\mathcal{X}$. The results indicated a good correspondence between the actual force $\mathbf{f}_a$ and the desired values when the desired force did not exceed 20 mN; the force percentage error was under 10%. In particular, the best distribution of force percentage error was obtained when the desired force range was [5 and 10 mN], i.e., the force percentage error was under 3%.
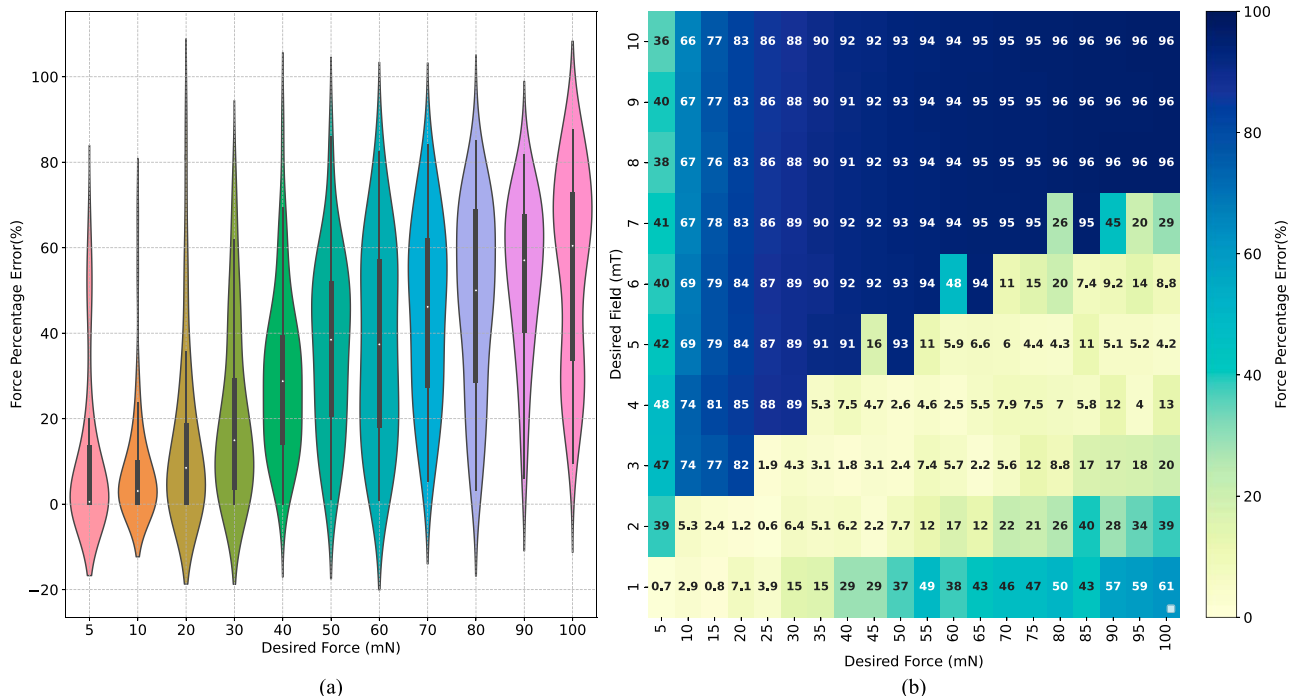
In addition, we also investigated the force percentage error distribution when the desired field range was [5 and 10 mN], as depicted in Fig. 3(b). To illustrate performance of our method, the median of force percentage error distribution across all 50 direction vectors was calculated for each desired field and force. One can note that when the desired field increases, a large desired force should be considered to obtain a lower force percentage error. This can be explained by the fact that once a magnetic robot's applied field and dipole moment are determined, the actual force is limited to a reasonable range under the defined CCS $\mathcal{X}$. Moreover, the Yoshikawa manipulability metric of each robotic arm was considered during the optimization, and some ill-conditioned joint configurations were not permitted, negatively affecting the force percentage error. As depicted in Fig. 4, this compares the median of force percentage error distribution with and without the robotic arms' Yoshikawa manipulability during optimization; the desired field amplitude was 1 mT. This also implies that the Yoshikawa manipulability metric is explored and enhanced at the expense of the force control error.

E. Analysis

The analysis of the field-priority force control provides insights into how to control the field and force using the three-coil REMA platform. Two main limiting factors that impede the decrease in the field percentage error. The first is the constraints in terms of the CCS, which ensures collision-free manipulations. The other is related to the Yoshikawa manipulability for each robotic arm. As one of the optimization objective functions, the Yoshikawa manipulability may weaken the force control's accuracy but improve the manipulation workspace's range. A field can be chosen to decrease the force percentage error according to the field-force heat map to generate the desired force. For example, if one wants to impose a force with an amplitude of 50 mN on a magnetic robot with a unit dipole moment, applying a field with an amplitude of 3 mT can result in a lower force percentage error.

F. Simulation

The effectiveness of our proposed algorithm is initially validated through a simulation environment constructed using ROS software. The virtual capsule robot, as depicted in Fig. 5(a), is expected to track a reference path in a large workspace. To mimic the robot's motion in real environment, we consider its gravity and dynamics. Consequently, a vertical magnetic force was continuously applied to overcome the force of gravity on the capsule. When employing real-time adjustment of the coil configuration to track the reference path, the smoothness of the control procedure may be affected. Therefore, a tradeoff method was made to split the travel path into different segments according to its curvatures. At each segment, the corresponding coil configuration was generated using Algorithm 1 to produce the desired field and force. It should be noted that the fields will be turned off to avoid the unexpected motion of the capsule during the transition between the two different coil configurations, as it is difficult to regulate the motion of the three robotic

This article has been accepted for inclusion in a future issue of this journal. Content is final as presented, with the exception of pagination.

6   IEEE TRANSACTIONS ON INDUSTRIAL ELECTRONICS

Fig. 3. Performance of the field-priority force control method. (a) Violin plots represent the force percentage error distribution under the desired field 1 mT with desired force range [5 and 100 mN]. Width of each density curve corresponds with the approximate frequency of data points in each region. Small box plot in the middle of each density curve shows the ends of the first and third quartiles and central dot of the median. (b) Median distribution of force percentage error under desired field range [1 and 10 mT] with desired force range [5 and 100 mN].
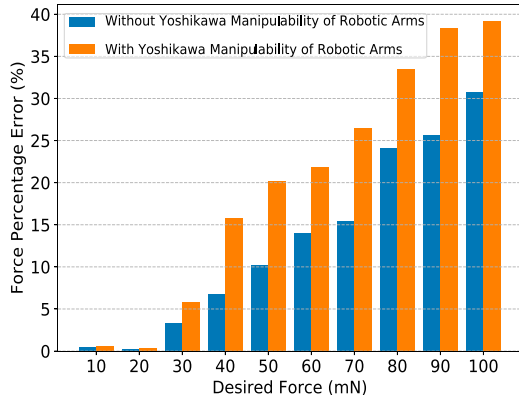
Fig. 4. Comparison of the median of field force percentage error distribution for considering and not considering the robotic arms' Yoshikawa manipulability when the desired field is 1 mT.

arms and the three-coil currents to maintain the expected field and force. The action of turning off the field will result in the robot experiencing a vertical downward displacement due to the influence of gravity. As shown in Fig. 5(a)–5(f) (Movie S1), the capsule robot successfully tracked the reference path using the field-priority force control method and Pure Pursuit path tracking algorithm.

IV. EXPERIMENTS AND RESULTS

To validate the performance of the proposed field-priority force control method for autonomous magnetic manipulations

using the REMA platform, we first established the REMA prototype employing three robotic arms (SJ-603-A, Anno Robot). Subsequently, several experiments were conducted, including navigating a catheter and propelling a mockup capsule. Moreover, a simulation environment for REMA was implemented for debugging and tuning relevant parameters by implementing these experiments. Please refer to the accompanying video for a visualization of the characteristic examples of the following experiments.

A. Experimental Setup

The developed REMA prototype consists of three mobile coils mounted on three independent six-DOF robotic arms for the generation of field and force in large workspaces (length × width × height: $450 \times 300 \times 350$ mm), as shown in Fig. 6(a). Each coil, equipped with a ferromagnetic core to enhance field strength, is fabricated with a weight of 1.2 kg. The system currently employs two orthogonally placed digital cameras (MER2-160-227U3C, DaHeng) to capture the top view and side view of the workspace, respectively. To achieve real-time control of the electric currents flowing into the coils, a control board STM32 serves as a low-level embedded controller to receive commanded electric current values from the master computer. Additionally, a customized ROS Visualization (RViz) interface was developed to provide researchers with a clear overview of the magnetic manipulation task execution. In addition, to magnetically actuate an unconstrained magnetic robot, a mockup capsule was designed and fabricated using resin through 3-D printing technology, as shown in Fig. 6(b), which
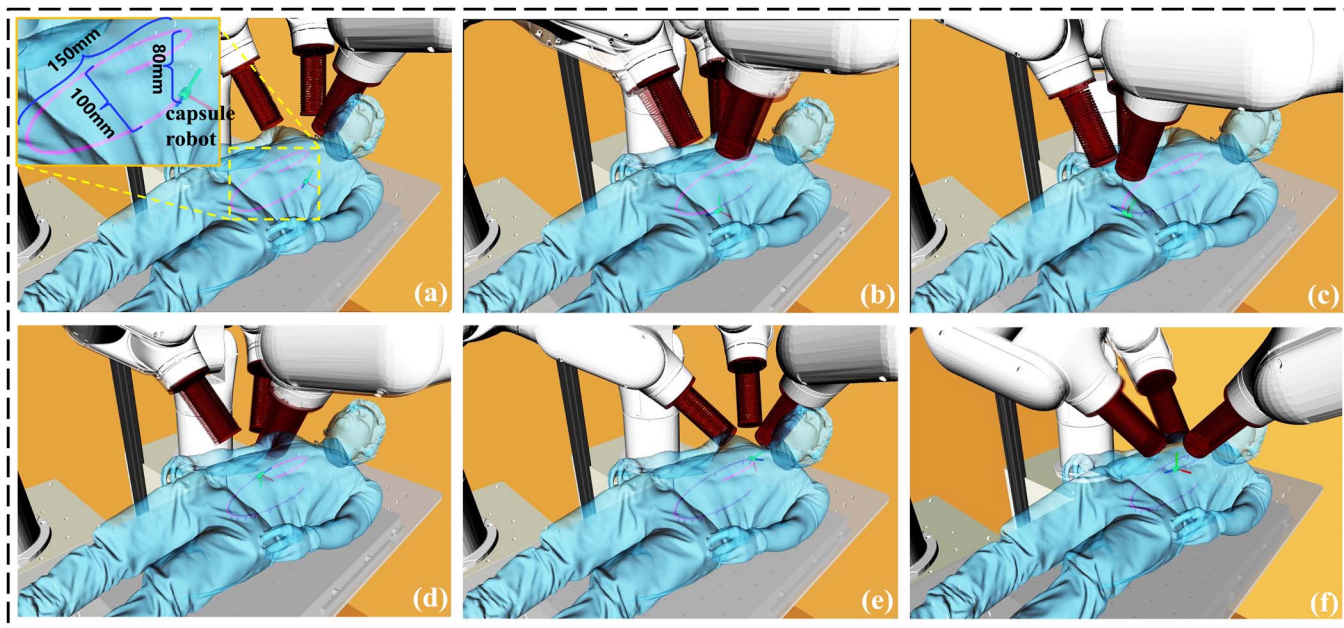
Fig. 5. Virtual capsule robot in simulation environment is magnetically propelled to track a 3-D helix path under the guidance of the field-priority force control method and Pure Pursuit path tracking algorithm (Movie S1). (a) $t=0$ s. (b) $t=20$ s. (c) $t=40$ s. (d) $t=60$ s. (e) $t=80$ s. (f) $t=100$ s.
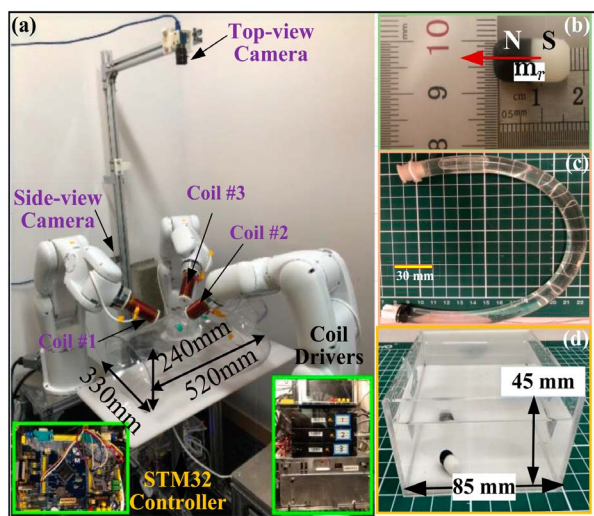

Fig. 6. Overview of the setup for the real-world experiments. Developed REMA prototype. (a) REMA comprises three mobile coils that are actuated by three independent six-DOF robotic arms. Low-level controller STM32 and three coil drivers are deployed to manipulate the electric currents flowing into coils. (b) Mockup capsule. (c) PVC tube phantom. (d) Cubic container phantom.

contains a magnet (diameter 4 mm and height 6 mm) with the dipole moment oriented parallel to its principal axis. To better mimic a tubular tissue in human body environments, a PVC tube with a 10-mm inner diameter [see Fig. 6(c)] was mounted on the human body model phantom. The tube was filled with 80% glycerol to imitate the environment with low Reynolds number. Moreover, in Fig. 6(d), a cubic container phantom filled with 80% glycerol was additionally utilized for actuating the capsule in a 3-D workspace. Although these phantoms are not

representative of actual medical scenarios, they are sufficient for our proof-of-concept experiments. Considering the movement speed of the magnetic robot is slower than that of robotic arms, the motion resolution of each robotic arm is set to 3 mm, that is, when the position variation of the magnetic robot exceeds 3 mm, the robotic arms will track its latest position. This could reduce the computation resources caused by real-time trajectory planning of the robotic arms.

B. Evaluation of Field-Priority Force Control Method in 2-D Tubular Environments

To assess the performance of the proposed field-priority force control method, a demonstration of propelling a mockup capsule in a C-shaped PVC tube was implemented. Specifically, the tube was fixed to the inner wall of the human–body model phantom, as shown in Fig. 7(a). The field-priority force control method could guarantee the capsule heading along the centerline of the tube via the desired fields and generate propulsive forces to propel the capsule to travel through the tube. Indeed, the desired field and force have the same direction vectors, aligned to the centerline of the tube.

The experimental results are exhibited in Fig. 7(a)–7(f) (Movie S2). During the actuation, the desired heading of the capsule was calculated according to the current position $\mathbf{p}_w$ for heading control, that is, to align it with the centerline of the tube. Otherwise, the capsule may become stuck owing to the constraints of the inner wall of the tube. It must be clarified that the transitioning from one coil configuration to another requires time (sometimes over 2 s), which depends on the trajectory execution time of the robotic arms. For example, the configuration transition for the coil shown in Fig. 7(a) to that in Fig. 7(b) (real-world view), takes approximately 3 s for the
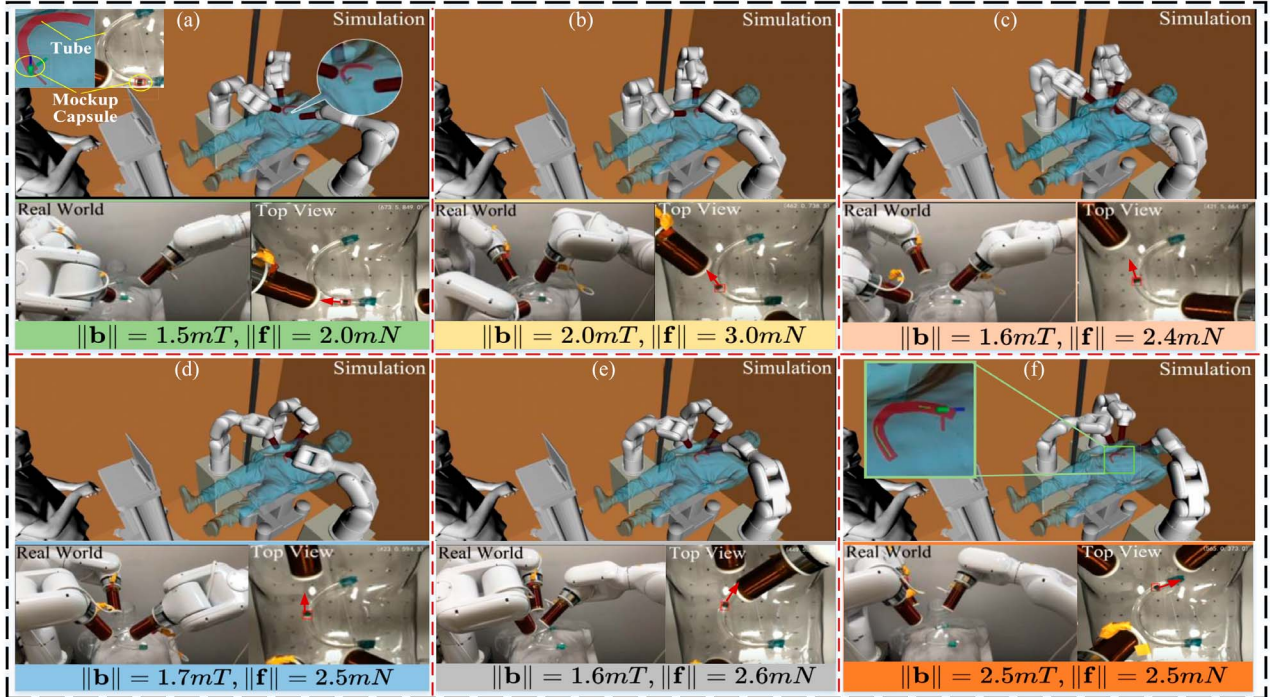
Fig. 7. Capsule is magnetically propelled through a C-shaped tube under the guidance of the field-priority force control method (Movie S2). Six combinations of field and force are applied to propel the capsule, thus moving through the C-shaped tube. Simulation environment and real-world view exhibit the real-time capsule's poses and the corresponding coil configurations. Red arrow in the top view indicates the capsule's heading direction. (a) $t = 0$ s. (b) $t = 18$ s. (c) $t = 30$ s. (d) $t = 38$ s. (e) $t = 46$ s. (f) $t = 70$ s.

robotic arms to adjust their poses. Although the motion speed of the robotic arms can be adjusted to a higher value, this may cause chattering and security risks. The results indicated that six combinations of field and force were successfully applied to propel the capsule to travel through the tube. Fig. 7(f) shows the traveled path of the capsule in the simulation environment.

C. Evaluation of Field-Priority Force Control Method in 3-D Spaces

To further demonstrate the efficiency of the proposed field-priority force control method, we conducted an experiment that enabled a capsule to track a planned path in the 3-D space under different heading directions. The capsule was submerged and levitated in a cubic container filled with 80% glycerol. Both the top-view and side-view cameras were used to track the 3-D position of the capsule.

Fig. 8 shows the experimental results of the capsule following an N-shaped path in a cubic container, with the heading pointing in the given directions (Movie S3). The whole experiment was conducted in three motion stages. Specifically, for Motion Stages I and III, the desired force direction vector did not align with the field direction vector, that is, the heading direction is inconsistent with the motion direction. A corresponding coil configuration was generated according to the planned path to produce the desired field and force during each motion stage. The moving speed of the capsule depends primarily on the magnitude of the applied force, which must be decreased before approaching the next motion stage.

In particular, when the field and force direction vectors remain unchanged, the variation in the field and force magnitudes with the same scaling factor can be obtained by tuning only the electric currents under the same coil configuration. We used the proportional-integral-derivative method to calculate the scaling factor based on the real-time position of the capsule, thus simultaneously modulating the amplitudes of the field and force. Under the guidance of this control strategy, we observed that the capsule could follow the planned path in the three motion stages, as shown in Fig. 9. In addition, the proposed field-priority force control method was proved effective in finding a good tradeoff between field-force generation and the manipulability of the three robotic arms. With respect to our REMA platform and the control strategy, the experiments presented herein demonstrated the effectiveness of steering a capsule in 3-D spaces.

V. DISCUSSION

The main limitation of the field-priority force control method is the difficulty in achieving the desired field and force control in the transition phase of different coil configurations. However, increasing the control frequency and velocity of the robotic arms can shorten the required time of the transition phase. However, the pulsatile liquid flow that existed in physiological environments still poses considerable challenges to the current algorithm. To overcome this limitation, a possible solution is to explore the mapping between the wrench and joint space of the three robotic arms, which can be achieved
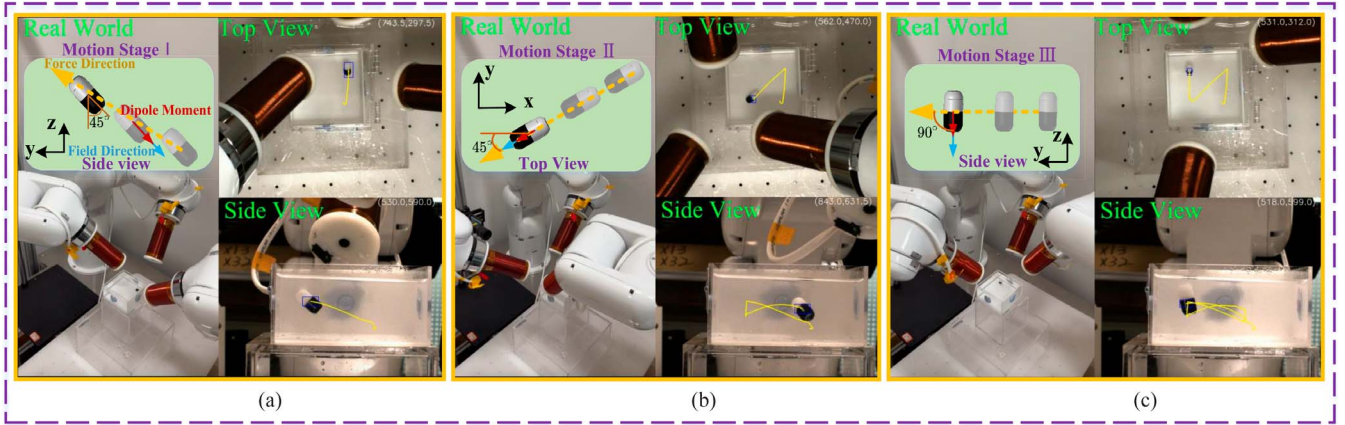
Fig. 8. Results of magnetically steering a mockup capsule under the guidance of the field-priority force control method to track an N-shaped path in 3-D spaces (Movie S3). The overall process is divided into three motion stages. (a) Motion Stage I with the capsule heading maintaining 45° with respective to the gravity direction, and the force along the y–z plane ($t = 30$ s). (b) Motion Stage II wherein the angle between the capsule's heading and the force direction is the same ($t = 60$ s). (c) Motion Stage III wherein the capsule heading maintains vertical (along the negative z-axis) and the force along the y-axis ($t = 80$ s).
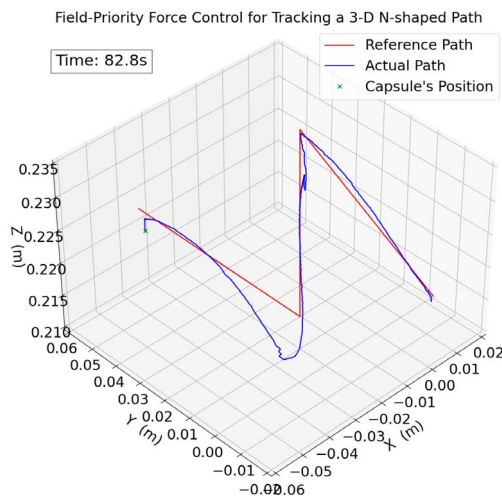

Fig. 9. Results of 3-D N-shaped path tracking.

using the differential method. Moreover, learning-based techniques can be used to improve the precise motion control [25]. In a previous study [26], we developed a reinforcement learning method for magnetic robots to reject unknown flow rates. Moreover, the designed simulation environment can provide a training environment for reinforcement learning to produce a robust policy.

Most current designs of EMA system with multiple coils are primarily limited to the confined workspace, the bulky or complex configuration, as well as the rapid decay of the magnetic field strength caused by the distance increase. Moreover, some potential issues impeding enlarging the coils include increases in inductance and the resistive heating in coils that requires a cooling system to mitigate [27]. Therefore, the construction of stationary EMA systems with human-scale workspaces remains a major challenge. Additionally, we will

conduct comprehensive real-word experiments involving more complex trajectories in various directions over a wider area.

VI. CONCLUSION

In summary, we introduced a novel magnetic field and force control method using a mobile EMA platform. We investigated the number of mobile coils required for the combined field and force generation. To ensure the dexterity of field and force control, a three-coil configuration was applied to manage a rich combination of fields and forces while providing a large workspace using a REMA system equipped with three robotic arms. Subsequently, a field-priority force control method was proposed to generate a Pareto-optimized coil configuration to guarantee the field control and optimize the actual force to a given value with acceptable errors while enhancing the Yoshikawa manipulability measure for each robotic arm. The REMA prototype was developed using three six-DOF robotic arms for autonomous control of magnetic robots in large workspaces. Validation experiments highlighted the dexterity and effectiveness of magnetic manipulation. We will develop advanced control strategies to enhance the efficiency and safety of autonomous robot navigation using our system in a dynamic environment.

REFERENCES

[1] P. E. Dupont et al., "A decade retrospective of medical robotics research from 2010 to 2020," *Sci. Robot.*, vol. 6, no. 60, Nov. 2021, Art. no. eabi8017.

[2] Z. Cai, Y. Qin, and J. Han, "Design and control of a miniaturized magnetic-driven deformable capsule robot for targeted drug delivery," *IEEE Trans. Ind. Electron.*, vol. 71, no. 8, pp. 9150–9160, Aug. 2024, doi: 10.1109/TIE.2023.3314843.

[3] M. Sitti et al., "Biomedical applications of untethered mobile milli/microrobots," *Proc. IEEE*, vol. 103, no. 2, pp. 205–224, Feb. 2015.

[4] T. Xu, G. Hwang, N. Andreff, and S. Régnier, "Planar path following of 3-D steering scaled-up helical microswimmers," *IEEE Trans. Robot.*, vol. 31, no. 1, pp. 117–127, Feb. 2015.

[5] Y. Cao et al., "Magnetic continuum robot with intraoperative magnetic moment programming," *Soft Robot.*, vol. 10, no. 6, pp. 1209–1223, Dec. 2023, doi: 10.1089/soro.2022.0202.

[6] J. W. Martin et al., "Enabling the future of colonoscopy with intelligent and autonomous magnetic manipulation," *Nature Mach. Intell.*, vol. 2, no. 10, pp. 595–606, Oct. 2020.

[7] F. Kong, Y. Zhu, C. Yang, H. Jin, J. Zhao, and H. Cai, "Integrated locomotion and deformation of a magnetic soft robot: Modeling, control, and experiments," *IEEE Trans. Ind. Electron.*, vol. 68, no. 6, pp. 5078–5087, Jun. 2021.

[8] S. Salmanipour and E. Diller, "Eight-degrees-of-freedom remote actuation of small magnetic mechanisms," in *Proc. IEEE Int. Conf. Robot. Automat.*, 2018, pp. 3608–3613.

[9] J. Sikorski, C. M. Heunis, F. Franco, and S. Misra, "The ARMM system: An optimized mobile electromagnetic coil for non-linear actuation of flexible surgical instruments," *IEEE Trans. Magn.*, vol. 55, no. 9, pp. 1–9, Sep. 2019.

[10] A. J. Petruska and J. J. Abbott, "Omnimagnet: An omnidirectional electromagnet for controlled dipole-field generation," *IEEE Trans. Magn.*, vol. 50, no. 7, pp. 1–10, Jul. 2014.

[11] S. L. Charreyron, Q. Boehler, B. Kim, C. Weibel, C. Chautems, and B. J. Nelson, "Modeling electromagnetic navigation systems," *IEEE Trans. Robot.*, vol. 37, no. 4, pp. 1009–1021, Aug. 2021.

[12] Q. Boehler, S. Gervasoni, S. L. Charreyron, C. Chautems, and B. J. Nelson, "On the workspace of electromagnetic navigation systems," *IEEE Trans. Robot.*, vol. 39, no. 1, pp. 791–807, Feb. 2023.

[13] Z. Yang, L. Yang, M. Zhang, N. Xia, and L. Zhang, "Ultrasound-guided wired magnetic microrobot with active steering and ejectable tip," *IEEE Trans. Ind. Electron.*, vol. 70, no. 1, pp. 614–623, Jan. 2023.

[14] M. P. Kummer et al., "OctoMag: An electromagnetic system for 5-DOF wireless micromanipulation," *IEEE Trans. Robot.*, vol. 26, no. 6, pp. 1006–1017, Dec. 2010.

[15] A. J. Petruska and B. J. Nelson, "Minimum bounds on the number of electromagnets required for remote magnetic manipulation," *IEEE Trans. Robot.*, vol. 31, no. 3, pp. 714–722, Jun. 2015.

[16] R. Chen, D. Folio, and A. Ferreira, "Mathematical approach for the design configuration of magnetic system with multiple electromagnets," *Robot. Auton. Syst.*, vol. 135, Jan. 2021, Art. no. 103674.

[17] A. W. Mahoney and J. J. Abbott, "Five-degree-of-freedom manipulation of an untethered magnetic device in fluid using a single permanent magnet with application in stomach capsule endoscopy," *Int. J. Robot. Res.*, vol. 35, no. 1–3, pp. 129–147, 2016.

[18] G. Pittiglio et al., "Collaborative magnetic manipulation via two robotically actuated permanent magnets," *IEEE Trans. Robot.*, vol. 39, no. 2, pp. 1407–1418, Apr. 2023, doi: 10.1109/TRO.2022.3209038.

[19] L. Yang, X. Du, E. Yu, D. Jin, and L. Zhang, "Deltamag: An electromagnetic manipulation system with parallel mobile coils," in *Proc. IEEE Int. Conf. Robot. Automat.*, 2019, pp. 9814–9820.

[20] X. Du, L. Yang, J. Yu, K. F. Chan, P. W. Y. Chiu, and L. Zhang, "Robomag: A magnetic actuation system based on mobile electromagnetic coils with tunable working space," in *Proc. 5th IEEE Int. Conf. Adv. Robot. Mechatron.*, 2020, pp. 125–131.

[21] S. Hwang, A. Ramos-Sebastian, and S. H. Kim, "Feedbackless automatic control of magnetic milli/microrobots: Generation and control of a trapping point using a single coil electromagnetic system," *IEEE/ASME Trans. Mechatronics*, vol. 27, no. 5, pp. 2997–3007, Oct. 2022.

[22] L. Yang, M. Zhang, Z. Yang, and L. Zhang, "Multimode control of a parallel-mobile-coil system for adaptable large-workspace microrobotic actuation," *IEEE/ASME Trans. Mechatronics*, vol. 28, no. 3, pp. 1662–1673, Jun. 2023.

[23] N. Gunantara, "A review of multi-objective optimization: Methods and its applications," *Cogent Eng.*, vol. 5, no. 1, Jul. 2018, Art. no. 1502242.

[24] K. Deb, A. Pratap, S. Agarwal, and T. Meyarivan, "A fast and elitist multiobjective genetic algorithm: NSGA-II," *IEEE Trans. Evol. Comput.*, vol. 6, no. 2, pp. 182–197, Apr. 2002.

[25] M. E. Tiryaki, S. O. Demir, and M. Sitti, "Deep learning-based 3D magnetic microrobot tracking using 2D MR images," *IEEE Robot. Autom. Lett.*, vol. 7, no. 3, pp. 6982–6989, Jul. 2022.

[26] M. Cai et al., "Deep reinforcement learning framework-based flow rate rejection control of soft magnetic miniature robots," *IEEE Trans. Cybern.*, vol. 53, no. 12, pp. 7699–7711, Dec. 2023, doi: 10.1109/TCYB.2022.3199213.

[27] C. Chautems and B. J. Nelson, "The tethered magnet: Force and 5-DOF pose control for cardiac ablation," in *Proc. IEEE Int. Conf. Robot. Automat.*, 2017, pp. 4837–4842.

Mingxue Cai (Member, IEEE) received the Ph.D. degree in control theory and control engineering from the Institute of Automation, Chinese Academy of Sciences, Beijing, China, in 2020.

He was a Postdoctoral Fellow with The Chinese University of Hong Kong, Hong Kong, China, from 2021 to 2023. He is currently working with the Guangdong Provincial Key Laboratory of Robotics and Intelligent System, Shenzhen Institute of Advanced Technology, Chinese Academy of Sciences, Shenzhen, China. His research interests include robotics, intelligent control, and deep reinforcement learning.

Zhaoyang Qi (Student Member, IEEE) received the bachelor's and master's degrees in instrument science and technology from Hefei University of Technology and the University of Science and Technology of China, Hefei, China, in 2018 and 2021, respectively. He is currently working toward the Ph.D. degree with the Department of Mechanical and Automation Engineering, The Chinese University of Hong Kong, Hong Kong, China, since 2022.

His research interests include development and control of electromagnetic systems and magnetic microrobotics.

Yanfei Cao received the B.E. degree in mechanical engineering and automation and the M.E. degree in mechanical and electronic engineering from the Nanjing University of Aeronautics and Astronautics, Nanjing, China, in 2016 and 2019, respectively. He is currently working toward the Ph.D. degree with the Department of Mechanical and Automation Engineering, The Chinese University of Hong Kong, Hong Kong, China.

His research interests include magnetic actuation, soft materials, and machine learning for medical robots.

Xinyu Wu (Senior Member, IEEE) received the B.E. and M.E. degrees in automation and computer engineering from the Department of Automation, University of Science and Technology of China, in 2001 and 2004, respectively, and the Ph.D. degree in automation and computer engineering from The Chinese University of Hong Kong, Hong Kong, in 2008.

He is currently a Professor with Shenzhen Institute of Advanced Technology, Shenzhen, China, and the Director of Center for Intelligent Bionic, Shenzhen, China. He has published over 180 papers and two monographs. His research interests include computer vision, robotics, and intelligent system.

Prof. Wu is an Associate Editor of IEEE TRANSACTIONS ON SYSTEMS, MAN, AND CYBERNETICS: SYSTEMS and IEEE ROBOTICS AND AUTOMATION LETTERS.

Tiantian Xu (Senior Member, IEEE) received the M.S. degree in industrial engineering from Ecole Centrale Paris, Paris, France, the Engineer degree (M.S. degree) in mechanic from Supmeca, Saint-Ouen, France, in 2010, and the Ph.D. degree in robotic engineering from the Institute of Intelligent Systems and Robotics (ISIR), University of Pierre and Marie Curie, Paris, in 2014.

She worked as a Postdoctoral Fellow for The Chinese University of Hong Kong, Hong Kong, China, from 2014 to 2016. She is currently working with the Guangdong Provincial Key Laboratory of Robotics and Intelligent System, Shenzhen Institute of Advanced Technology, Chinese Academy of Sciences, Shenzhen, China. Her research interests are currently focused on design and control of magnetic actuated helical microswimmers.

Li Zhang (Fellow, IEEE) received the Ph.D. degree in physics from the University of Basel, Basel, Switzerland, in 2007.

He was a Postdoctoral Fellow and a Senior Scientist with the Institute of Robotics and Intelligent Systems (IRIS), Swiss Federal Institute of Technology (ETH), Zürich, Switzerland, from 2007 to 2012. He is currently an Associate Professor with the Department of Mechanical and Automation Engineering, The Chinese University of Hong Kong, Hong Kong, China. His research interests include microrobotics and nanorobotics for biomedical applications and their collective behaviors for the development of intelligent robot swarms at small scales.

Dr. Zhang received the Hong Kong Research Grants Council (RGC) Early Career Award in 2013 and several awards from IEEE conferences. He is also a Distinguished Lecturer appointed by the IEEE Nanotechnology Council (IEEE NTC).